Magnetospheric and ionospheric response to a substorm: Geotail HEP-LD and Polar PIXIE observations

S. Håland,[1] N. Østgaard,[1] J. Bjordal,[1] J. Stadsnes,[1] S. Ullaland,[1,2]
B. Wilken,[3]
T. Yamamoto,[4,5]
T. Doke,[6]
D. L. Chenette,[7]
G. K. Parks,[8] M. J. Brittnacher,[8]
G. D. Reeves[9]

Accepted for publ. in J. Geophys. Res., May 1999

Abstract. The High Energy Particle - Low energy particle Detector experiment (HEP-LD) on board the Geotail spacecraft and the Polar Ionospheric X-ray Imaging Experiment (PIXIE) on board the Polar satellite have been used to examine a substorm event. On December 10, 1996, around 1700 UT, a substorm event with two onsets took place. The event occurred during a weak magnetic storm that started on December 9. Several of the classical substorm features were observed during the event: reconnection and neutral-line formation in the near-Earth geomagnetic tail, injection of energetic particles at geosynchronous orbit, and particle precipitation into the ionosphere. Magnetic field line mapping of the energetic precipitation area into the geomagnetic tail shows that the substorm development on ground is closely correlated with topological changes in the near-Earth tail. In the first onset, mainly soft electrons are involved, with only a transient energetic precipitation delayed relative to the onset. The second onset about 30 min later includes both soft and energetic electrons. The source regions of both onsets are found to be located near the earthward edge of the plasma sheet, while the source region of the transient energetic precipitation during the first onset is in the distant tail. Magnetic reconnection occurs sporadically and burst-like before the onsets. Both onsets appear to be triggered by northward turning of the interplanetary magnetic field. The study also demonstrates that the concept of pseudobreakups should be used with care unless global observations are available.

1. Introduction

The International Solar Terrestrial Physics (ISTP) program gives a unique opportunity to get a global view of substorm events. In this paper, we focus on the measurements from the High Energetic Particle - Low energy particle Detector experiment (HEP-LD) and magnetic field observations by Geotail in the near-Earth tail (25 R_E downtail), compared with the global images of the electron precipitation provided by the Polar Ionospheric X-ray Imaging Experiment (PIXIE) and the Far Ultraviolet Imager (UVI) on board the Polar spacecraft during a substorm event on December 10, 1996. Additional information about the substorm development is obtained from satellites in geosynchronous orbit, interplanetary magnetic field (IMF) monitors in the solar wind and ground based magnetometers. A still unresolved problem in substorm physics is the cause of the sudden onset and the location of the initial disruption area.

One of the main theories, the near-Earth neutral line (NENL) model [*Hones*, 1976, 1977] suggests that substorm onset is closely associated with magnetic reconnection and the formation of a magnetic neutral line in the near-Earth magnetotail (X_{GSM} in the range -15 R_E to -25 R_E). As a result of the reconnection process, it is believed that parts of the plasma sheet are pinched off and propagate tailward as a plasmoid. Although a significant part of the energy accumulated during the growth phase escapes through the plasmoid, a substantial amount of energy is released when the remaining plasma is accelerated earthward. Recent developments of the NENL model [e.g., *Baker et al.*, 1996; *Shiokawa et al.*, 1998], also take into account some of the apparent shortcomings of the original model; timing of the observations, large-scale mapping and onset mechanisms.

The X line and the escaping plasmoid produce characteristic signatures in the plasma and magnetic field. Tailward of the reconnection site, these features are often observed as a bipolar signature in the B_Z component of the magnetic field and fast tailward plasma flow [*Scholer et al.*, 1984a; 1984b; *Richardson and Cowley*, 1985]. The bipolar B_Z is often accompanied by a strong core field, observed as a strong deflection of the B_Y component [*Slavin et al.*, 1989; 1995]. Such observations support the idea of helical-shaped three-dimensional flux ropes rather than the conventional two-dimensional plasmoid picture.

Substorms are characterized by a rapid increase in the flux of energetic particles, an injection [e.g., *Erickson et al.*, 1979] together with a reconfiguration of the magnetic field, a dipolarization [e.g., *Kokubun and McPherron*, 1981]. These features are frequently observed by spacecraft in geosynchronous orbit and are therefore recognized as reliable indicators for substorm onset. The dipolarization of the magnetic field is often interpreted as a sudden decrease in the cross-tail current intensity, a current disruption. The disrupted tail current is thought to be converted into field aligned currents (FAC) which are closed via a loop into the iono-

[1]Department of Physics, University of Bergen, Norway.
[3]Max-Planck-Institut für Aeronomie, Katlenburg-Lindau, Germany.
[4]Institute of Space and Astronautical Science, Sagamihara, Japan.
[6]Advanced Research Institute for Science and Engineering, Waseda University, Shinjuku-ku, Tokyo, Japan.
[7]Lockheed-Martin Advanced Technology Center, Palo Alto, California.
[8]Geophysics Program, University of Washington, Seattle, Washington.
[9]Los Alamos National Laboratory, Los Alamos, New Mexico.
[5]Deceased February 20, 1998.
[2]Deceased October 10, 1998.

sphere. The current diversion creates a substorm current wedge (SCW) which expands both azimuthally and radially. The location of the initial current disruption associated with the global substorm is now believed to be in the near-Earth region (within 15 R_E) [*Ohtani et al.*, 1990 and references therein].

Some authors [e.g., *Lui*, 1991] argue that the reconnection of the last closed field line occurs 5-30 min after the explosive onset. In this scenario, substorms are initiated by some local instability and current disruption near the inner edge of the plasma sheet at radial distances within 10 R_E [see e.g., *Lui*, 1996 and references therein]. The reconnection is then attributed to a tailward propagating rarefaction wave and is regarded as a secondary effect. It is therefore still debated whether reconnection is a cause or a consequence in the substorm sequence.

Most substorms can be related to disturbances in the solar wind [see e.g., *Kokubun et al.*, 1977; *Spence*, 1996]. In works by *Lyons* [1995, 1996], it is claimed that all substorms are triggered by disturbances in the IMF, whereas others [e.g., *Henderson et al.*, 1996; *Angelopoulos et al.*, 1996] have discussed events without any direct solar wind triggering.

In the ionosphere the substorm is observed as particle precipitation over a broad energy range and is visualized through the "auroral substorm" [*Akasofu*, 1964]. Precipitating electrons deposit their energy into the atmosphere by ionization, excitation, heating of the neutral gas, and X-ray bremsstrahlung. The onset of the substorm will be observed as a rapid increase in all these processes. While most of the energy deposition involves both primary and secondary electrons over a wide energy range, the X rays are produced by high-energy electrons (in the energy range above a few keV) giving information on the energetic precipitation during substorms [*Robinson and Vondrak*, 1994].

After the explosive onset the auroral bulge expands both poleward and longitudinally. This corresponds to the azimuthal and radial expansion of the current wedge in the magnetosphere [*McPherron et al.*, 1973].

2. Instrumentation

Our primary data basis have been the HEP-LD instrument on board the Geotail spacecraft and the PIXIE X-ray camera on board the Polar spacecraft.

During the events studied here, the HEP-LD instrument was run in a special plasmoid mode. In this mode, HEP-LD measures energetic ions in 10 logarithmic spaced energy channels in the range 30 - 1500 keV. The spatial resolution is 16 azimuthal sectors and 3 polar look directions, covering the entire sphere during one 3-s spin. The instrument does not distinguish between different ion species in this particular mode; we are therefore not able to say anything about the origin of the particles. The energetic ion measurements provided by HEP-LD are particularly well suited for plasma sheet and boundary layer measurements, where the large gyroradius of the ions can be utilized for remote sensing of plasma boundaries [*Kettmann and Daly*, 1988; *Richardson et al.*, 1989] and for bulk flow measurements [*Richardson et al.*, 1987]. Further information about the HEP-LD sensor system can be found in the works of *Wilken et al.* [1993] and *Doke et al.* [1994].

The PIXIE camera provides images of the X-ray bremsstrahlung seen during substorms. It is assumed that the X-ray production occurs at about 100 km altitude. Even if the probability of generating an X-ray photon from an electron slowing down in the atmosphere increases as a function of the initial electron energy, a 200 keV electron only deposits 0.5% of its energy as X rays [*Berger and Seltzer*, 1972]. Nevertheless, these measurements provide an opportunity to study the global energetic electron precipitation, even in the Sun-lit area. The instrument is a pinhole camera with two proportional counters, detecting X rays in the energy range from 2 - 60 keV [*Imhof et al.*, 1995]. As the front chamber was turned off during this event only X-ray measurements above 10 keV were available for this study, and owing to the weakness of the event we detect X rays only in the energy range from 10 to 20 keV. Each image used in this paper presents 5-min accumulations of the radiation.

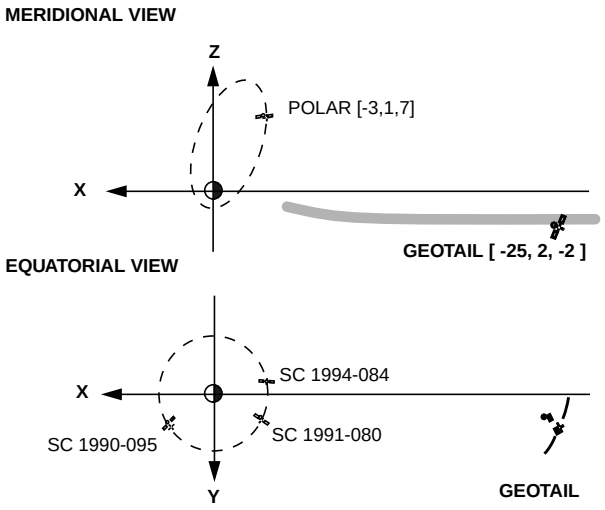

Figure 1. Spacecraft locations for Geotail, Polar, SC 1994-084, SC 1991-080, and SC 1990-095 around substorm onset of the event. The Wind spacecraft was located at [72, -41, 7 R_E GSM] upstream.

The UV imager on board the Polar satellite provides global images of emissions in the Lyman-Birge-Hopfields-Long (LBHL) band. This band is dominated by the emission created by the electron impact on N_2. All electron energies above the excitation energy (~7 eV) contribute in this process, and the intensity reflects the total energy influx of electron precipitation. As the lower energies usually dominate, the UVI provides the global features of the softer part of the electron distribution. For more information about the UVI, see *Torr et al.* [1995]. The exposure time for the images shown in this paper is 37 seconds.

Solar wind data and measurements of the IMF were available from the magnetic field experiment [*Lepping et al.*, 1995] and solar wind experiments [*Ogilvie et al.*, 1995] on board the Wind spacecraft, located upstream at [72, -41, 7 R_E GSM]. Data from geosynchronous altitude consist of energetic particle measurements from a set of satellites operated by Los Alamos National Laboratory (LANL). Two of the LANL satellites, SC 1991-080 and SC 1994-084 were favorably located in the midnight sector during the event. A third LANL satellite, SC 1990-095, was located in the early afternoon sector. The X-ray emissions observed by PIXIE are primarily generated by energetic electrons with energies above 20 keV [*Berger and Seltzer*, 1972]. We have therefore mainly focused on the lower-energy channels (50 - 500 keV) when we compare the ionospheric X-ray fluxes to particle injections seen by the LANL satellites. Figure 1 shows a meridional and an equatorial view of the locations of the various spacecraft whose data were used for the analysis.

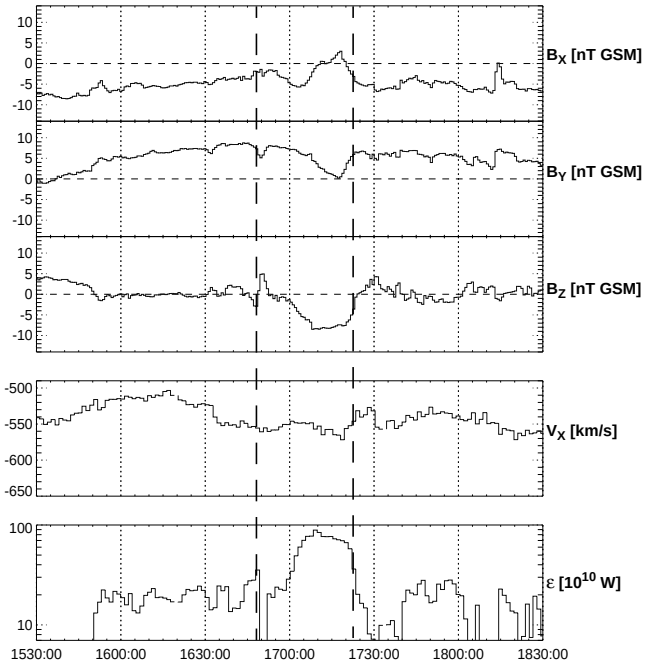

Figure 2. Magnetic field and solar wind velocity measured by the Wind spacecraft located at [72,-41, 7 R_E GSM]. The ε parameter (bottom) is derived from the magnetic field, the density and the bulk velocity. The rapid decrease in the ε parameter related to the northward turning of the IMF B_Z at 1648 and 1723 UT are indicated with dashed lines.

3. Observations: Overview

The substorm event discussed here was associated with a weak geomagnetic storm that started the day before. During the storm the *Dst* index reached a minimum of -32 nT. Around onset on December 10, the *Dst* index was -17 nT, and the *Kp* index was 4^+.

Solar wind conditions play an important role as input parameters for the magnetosphere-ionosphere interaction. The magnetic field, solar wind bulk speed, and the resulting ε parameter [*Akasofu*, 1981] during the investigated event are shown in Figure 2, where the dashed lines mark the northward turning of the IMF and the corresponding decrease in the ε parameter.

Using the time delay analysis described by *Sergeev et al*. [1986], we estimate the total propagation time between Wind and the front side magnetopause to be ~7 min. Another 2.5 - 9 min [*Kan et al.*, 1991] propagation time must be added to account for the time it takes for the convection changes caused by the solar wind at the magnetopause to reach the nightside plasma sheet. In total, this gives an expected time shift of ~10 - 16 min between the Wind measurements and the nightside magnetosphere. This time shift has been taken into consideration during the interpretation of the different observations.

Plate 1 shows key parameters from the Geotail HEP-LD instrument and the tail magnetic field during the event. The three upper panels show the magnetic field components in GSM coordinates. Panel 4 shows the differential flux of ions from the HEP-LD instrument and the lower panel shows the azimuthal directional distribution of the particles. Note that the vertical axis shows sensor look direction; increased count rates in the sun sector therefore represent a net bulk flow of particles tailward.

Figures 3a-3c show energetic particle measurements from the LANL satellites SC 1991-080 and SC 1994-084. Figure 3d shows the time development of the differential X-ray flux in the energy range 10 - 20 keV within a reference area in the upper atmosphere. The reference area (see Plate 2a) is delineated in the east-west direction by the local time sector 19.4 - 24 MLT and extends from 64˚ to 76˚ corrected geomagnetic (CGM) latitude in the north-south direction. The area was chosen to include both onsets but still avoid most of the eastward expansion, as we intend to focus on the initial injections related to the two onsets. The differential X-ray flux is accumulated for 5 min within the area. Repeating this procedure every 30 s and using the end of the interval as the time indicator, the temporal changes of the average differential flux in the area is found with an approximate resolution of about 30 s. It should be pointed out that flux values around 12 (kev s sr $cm^2)^{-1}$ in this plot corresponds to only 3 photons, such low area integrated fluxes should therefore be interpreted with care.

Magnetic pulsations within the Pi2 range are regarded as reliable signatures for substorms and are often used for timing of the onset. Figure 3e shows the magnetic pulsations (horizontal component) from Sodankylä.

Figure 4 shows ground magnetic signatures of the event from stations at midlatitude and low latitude in the nightside. The ground magnetic measurements have been utilized to obtain information about field-aligned currents and the current wedge development during the event. The left panel shows the D component (east-west) of the ground magnetic field, and right panel shows the H component (horizontal). Stations located in the northern hemisphere are shown in the upper part of the panels in an east-west arrangement where VAL represents the westernmost station. Stations located in the southern hemisphere are shown in the lower part of the figure in the same east-west arrangement where CZT represents the westernmost station. The location of the stations and estimated positions of field-aligned currents are also shown in Figure 5. Full names of the stations, CGM coordinates, and local time positions are given in Table 1.

Plate 2 shows a sequence of images from PIXIE during the period 1715-1800 UT. Each image is accumulated for 5 min and reflects the differential flux in the energy band from 10.0 to 20.0 keV. The rightmost column of the figures shows how the areas of X-ray emission map to the electron source area in the magnetosphere. The estimated source region is obtained by tracing each field line along a contour of the PIXIE image to the central plasma sheet (i.e., current sheet) in the magnetosphere. The contour delineating each image is determined by a predefined threshold level in the X-ray flux. The Tsyganenko T96 magnetic field model [*Tsyganenko*, 1995] is used to map the contour into the magnetosphere. Input parameters for the T96 model are taken from the Wind satellite, and the Wind measurements have been shifted ~7 min in time to represent the conditions on the subsolar magnetopause.

Plate 3 shows the UV images from 1643 to 1749 UT, displaying the patterns of the soft electron precipitation into the ionosphere during the substorm event. Each image has an exposure time of 37 s and shows the total number of photons. The time given above each image represents the center time.

The observations from Geotail and Polar can be separated into a set of stages and combined with the additional observations from the solar wind and geosynchronous altitude to form a consistent picture of the substorm events. We will therefore present the observations chronologically.

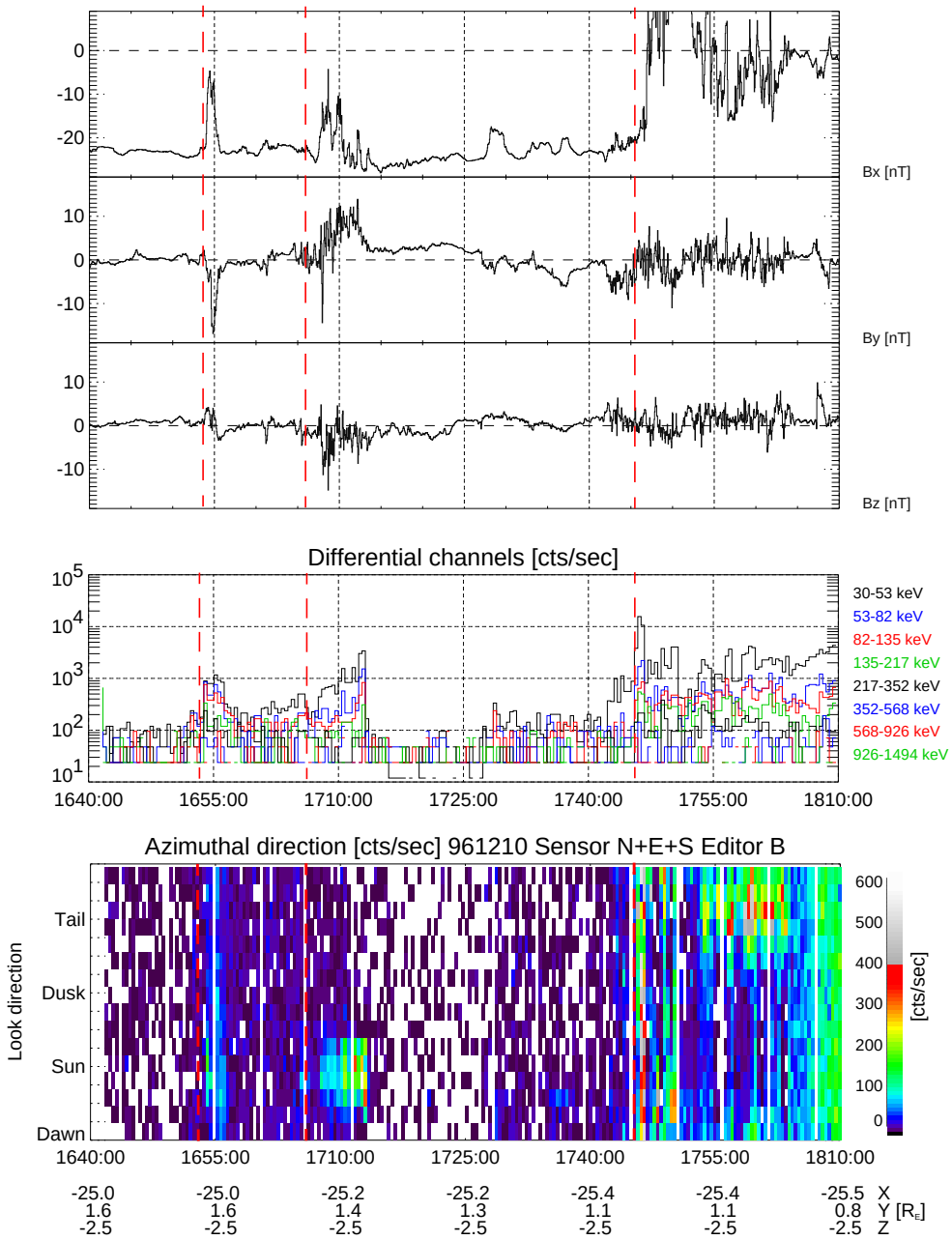

Plate 1 HEP-LD key parameters and magnetic field measurements from the Geotail spacecraft. The reconnection signatures at 1654 and 1704 UT and the reentry into the dense plasma sheet at about 1746 UT are indicated by vertical dashed lines.

3.1. Prior to 1650 UT

Geotail was located around 25 R_E downtail, near midnight in the tail and close to the current sheet during the event. The magnetic field is stronger and more stretched than predicted by models - a configuration often observed during the growth phase of a substorm. Figure 3d reveals a small enhancement in the X-ray flux from ~1640 UT, but the precipitation at this stage is too weak to be observed on the global images shown in Plate 2a. In the UV images (Plates 3a and 3b) we see growth phase signatures as a transpolar arc near midnight and diffuse aurora in the late morning and late evening sector.

The IMF B_Z component remains very close to zero for more than 1 hour prior to the first event, but owing to the rather high solar wind velocity and a clock angle of ~90˚ the energy input is still slightly above the threshold level for substorm onset at 10^{11} W [*Akasofu*, 1981].

3.2. At 1654 UT

At about 1654 UT, the HEP-LD instrument detects a short period of increased ion flux (Plate 1). The directional distribution shows a minor sunward/tailward anisotropy indicating tailward acceleration, but the effect is not very pronounced at this stage. Plasma data from the LEP instrument onboard Geotail [*Mukai et al.*, 1994] also reveals an approximately 2-min period of tailward flow (data not shown). Magnetic field measurements on

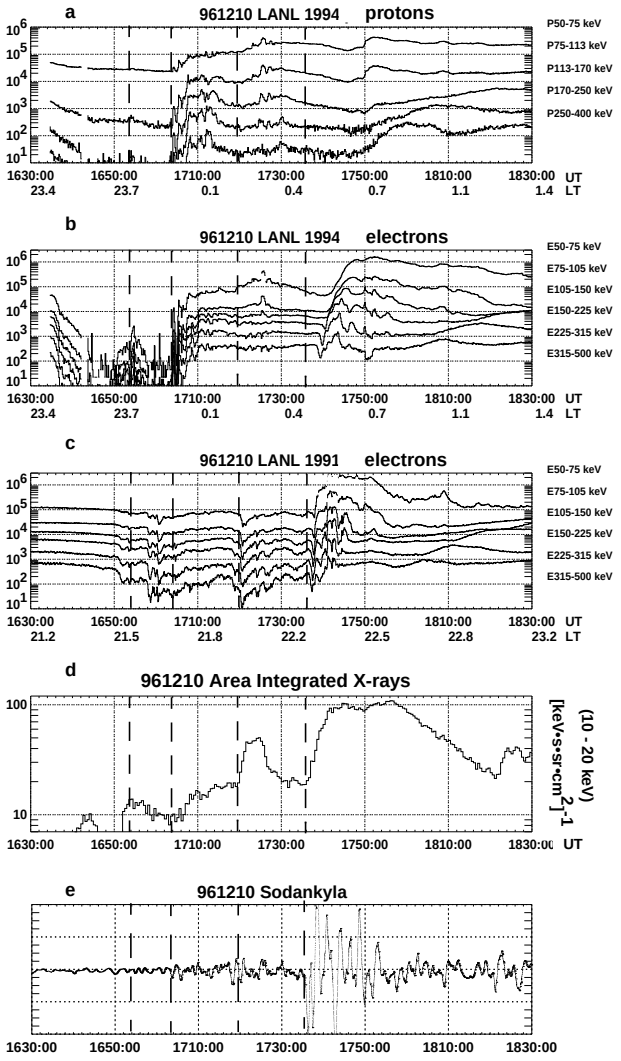

Figure 3. (a-c) The particle measurements from two of the LANL spacecrafts. (d) The area-integrated differential X-ray flux 10-20 keV in the region from 19.4 to 24.0 MLT and 62˚ to 76˚ magnetic latitude measured by PIXIE (the area is marked with a red box in Plate 2a, top). (e) Magnetic pulsation measurements from Sodankylä, Finland. Note that the pulsation data are given in normalized units. The first reconnection signature at Geotail at 1654 UT, the onsets at 1704 and 1736 UT and the transient increase of energetic precipitation at 1720 UT are marked with dashed lines.

Geotail show a typical bipolar B_Z signature and a strong peaked B_Y deflection. Together, these observations indicate a small burst-like reconnection event and possibly a tailward propagating flux rope.

There is a brief recovery in the electron flux at SC 1994-084 and a small drop in the electron flux at SC 1991-080 around 1652 UT. In the ionosphere a weak enhancement is seen in the area integrated X-ray flux from about 1648 UT (Figure 3d), but the flux is too low to be observed in the global X-ray images. Note that an X-ray flux of 12 (keV s sr cm^2)$^{-1}$ corresponds to only three photons; this enhancement may therefore be statistical fluctuations. No specific response to the reconnection event at 1654 is seen in the X rays. In the UV images (Plates 3c and 3d) a weak but distinct brightening is seen in the premidnight sector at that time. The brightening may be associated with the burst of reconnection.

In the ground magnetic measurements at midlatitude and low latitude (Figure 4), there are no signatures of field-aligned currents at 1654 UT, nor are there any significant response in the pulsation data from Sodankylä.

3.3. At 1704 - 1707 UT (First Onset)

On Geotail, a second, more pronounced interval of tailward streaming ions commences around 1704 UT and lasts for nearly 7 min. The interval of distinct tailward flow at Geotail is succeeded by a period of low flux which lasts until ~1742 UT.

An injection-like increase is seen at the geostationary SC 1994-084 at 1704 - 1707 UT. However, there is no net energization of the particles; the flux is merely returning to the level before 1635 UT. The apparent increase seen at SC 1994-084 is therefore most likely caused by a local plasma sheet movement or a reentry into the dense plasma sheet.

Again, we observe a small enhancement in the area integrated X-ray fluxes at 1707 UT, but the precipitation is too weak to be seen in the global X-ray images. The UV images (see Plate 3), however, show a significant, breakup like enhancement from Plate 3d to 3e. Plates 3f and 3g show that the UV intensity continues to increase and the bulge expands westward, eastward, and poleward during the subsequent period. The UV expansion is now centred around 2300 MLT. Pulsation data from Sodankylä (see Figure 3d) reveal a weak onset of pulsations around 1704 UT. We will therefore use the time 1704 UT as the first onset.

The ground magnetic signatures indicate a downward field-aligned current (downward FAC) at ~0400 MLT and an upward field-aligned current (upward FAC) at ~2300 MLT as illustrated in Figure 5. In the northern hemisphere, the stations MMB and LNP are just inside the current wedge; the positive horizontal component on both stations is a response to both downward FAC and upward FAC. The other stations are located west of the upward FAC; they show negative H perturbations and small positive D perturbations. In the southern hemisphere, only GNA is inside the current wedge; the H component is positive and there is no change in the D component. The stations AMS, PAF and CZT are all west of the SCW and respond to the upward FAC; negative D component and no change in the H component. EYR and CNB are east of the SCW and reflects primarily the downward FAC; positive D component and no H perturbation.

3.4. At 1720 UT

Around 1720 UT, there is a rapid increase in the area integrated X-ray flux. The global X-ray image generated for the time interval 1720 - 1725 UT (Plate 2b) shows a breakup like intensification of the precipitation. The enhancement takes place in the 2200 - 2300 MLT sector and at rather high latitudes (poleward of 70˚ CGM latitude). Note that the spot does not expand farther but fades away and disappears during the subsequent images.

The right-hand side of Plate 2b shows the source area for the spot. Although field line tracing during disturbed conditions and at such high latitudes are subject to severe distortions, the result indicates a source region tailward of Geotail. There are no distinct injection signatures at geosynchronous altitude at this stage, except for a small increase in the lower energy channels of the electron flux at SC 1994-084.

At Sodankylä, a stronger Pi2 signature is seen at 1717 UT, i.e., 3 min before this energetic precipitation event.

In the UV images, increasing intensity and features expanding

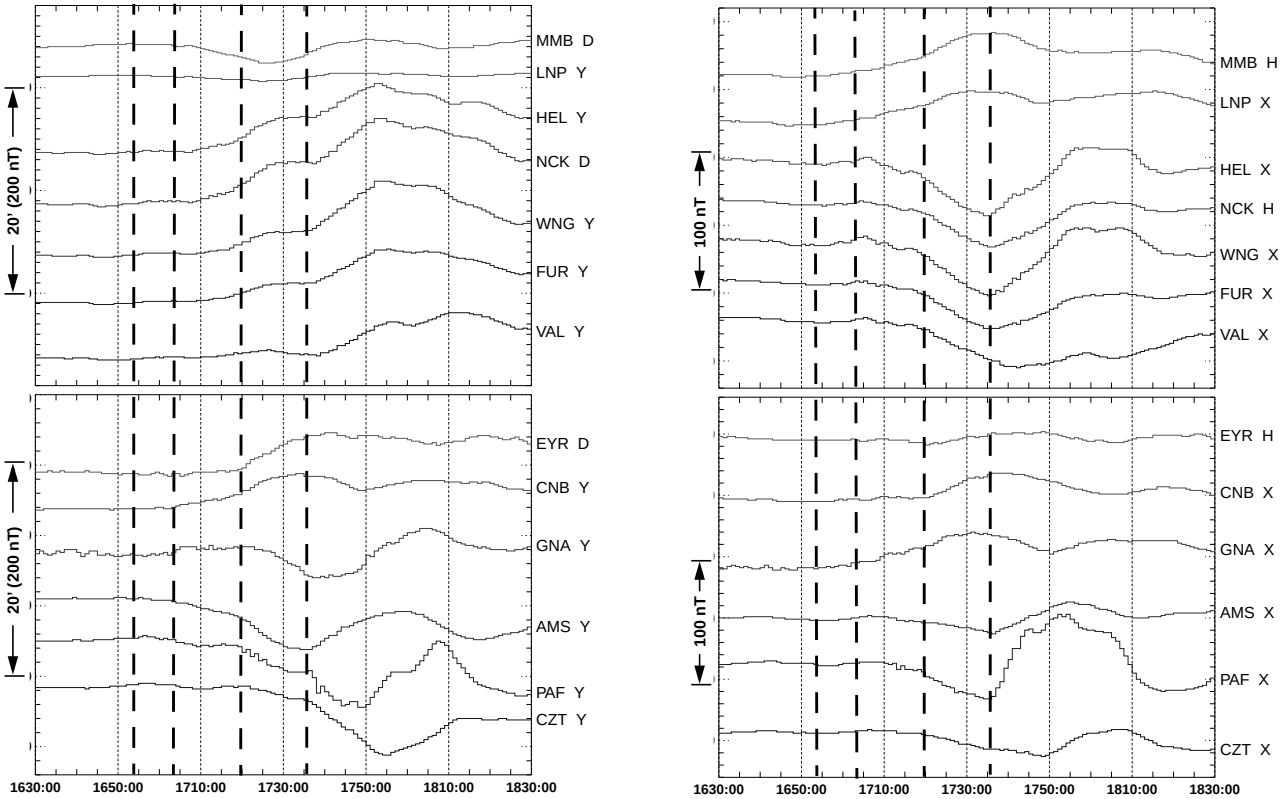

Figure 4. (left) East-west components of the ground magnetic field from selected stations in the northern hemisphere (top part of the plot) and the southern hemisphere (bottom part of the plot). (right) Horizontal components from the same set of stations. Note that some of the stations use a HDZ system where the east-west deflection is given in degrees, while the other stations use a XYZ coordinate system. The first reconnection signature at Geotail at 1654 UT, the onsets at 1704 and 1736 UT and the transient increase of energetic precipitation at 1720 UT are marked with dashed lines. Full names and CGM coordinates of the stations are given in Table 1. The locations of the stations are also indicated in Figure 5.

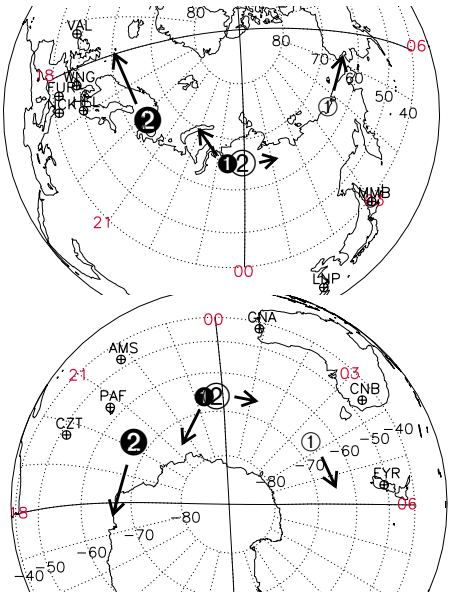

Figure 5. Location of the stations in the (top) northern hemisphere and the (bottom) southern hemisphere at 1730 UT. The FACs are shown by solid circles (upward) and open circles (downward) for the onsets at 1704 and 1736 UT numbered 1 and 2, respectively. The grid shows CGM longitudes and latitudes. The arrows indicate the inferred motion of the field aligned currents.

Table 1. Corrected Geomagnetic Coordinates and Magnetic Local Time Positions at 1730 UT for the Ground Magnetic Stations Shown in Figure 5.

Station	CGM Latitude	CGM Longitude	MLT at 1730 UT
Memambetsu, MMB	36.9	215.0	3.0
Lunping, LNP	17.9	192.8	1.4
Hel, HEL	50.6	95.3	18.9
Nagycenk, NCK	42.6	91.6	18.6
Wingst, WNG	50.0	87.0	18.3
Fürstenfeldbruck, FUR	43.4	87.0	18.3
Valentia, VAL	49.4	70.9	17.3
Eyrewell, EYR	-50.2	256.5	5.5
Canberra, CNB	-45.9	226.9	3.6
Gnagara, GNA	-44.4	186.5	1.0
Amsterdam Island, AMS	-49.1	138.4	21.8
Port Aux Francais, PAF	-58.5	121.9	20.7

CGM, corrected geomagnetic; MLT, magnetic local time; UT, universal time.

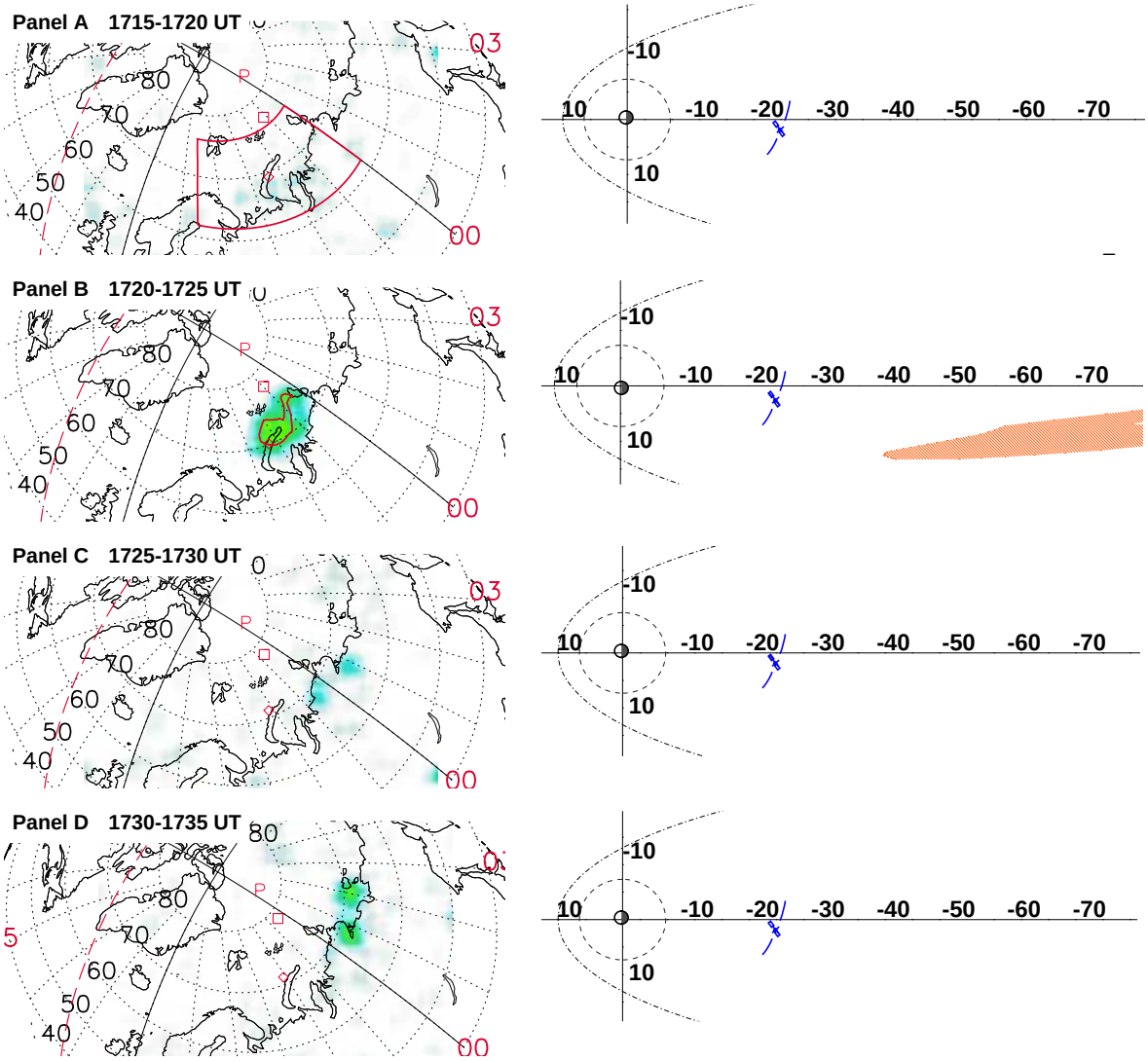

Plate 2 (eft) X-ray images from the PIXIE instrument; (right) corresponding source areas (of the red contour) in the magnetosphere. Each PIXIE image in this sequence represents a 5-min accumulation of the X-ray flux within the given time interval. The grid is CGM coordinates. Local time is labeled with red numbers. The source areas are mapped using the Tsyganenko T96 magnetic field model, parameterized with realistic solar wind input parameters. The reference area used for calculation of the area integrated differential fluxes is marked in Plate 2a. (e-h) Note that the mapping now places Geotail spacecraft within the source area, a view also supported by the measurements from Geotail.

both azimuthally and radially are seen, quite different from the observation of the energetic precipitation by PIXIE. The increase of the energetic precipitation seen by PIXIE seems to take place in the poleward edge of the UV features seen in Plate 3g. The first onset therefore seems to be dominated by precipitation of soft electrons.

The ground magnetic signatures shown in Figure 4 indicate movements and increases in the field-aligned currents. The upward FAC moves north and west, while the downward FAC moves eastward. The increase of the FACs is reflected in the larger perturbations of the magnetic field. The westward motion of the upward FAC can be inferred from the decrease in D without any H perturbation at the station AMS. Similarly, the eastward motion of the downward FAC can be seen from the negative D component at GNA and the positive H component at CNB which indicates that CNB is now inside the SCW. The movement is illustrated with arrows in Figure 5.

3.5. At 1736 UT (Second Onset)

The substorm associated injection of energetic particles is observed at 1736 UT. At this time, SC 1991-080 observes a nearly dispersionless injection (seen both in the ions and electrons. SC 1994-084 is located further east) the electron injection is therefore dispersed. No increase in the flux of ions is observed at SC 1994-084, until the current wedge has expanded eastward and reached the spacecraft around 1749 UT.

At PIXIE, the rapid increase in X-ray flux at 1736 marks the second onset of the substorm. Note that this breakup takes place further west (2000 - 2200 MLT) and equatorward (equatorward edge at 65˚) of the first onset. Field line tracing of the source area (see Plate 2e) demonstrates that the source region is much closer to the Earth during this latter breakup.

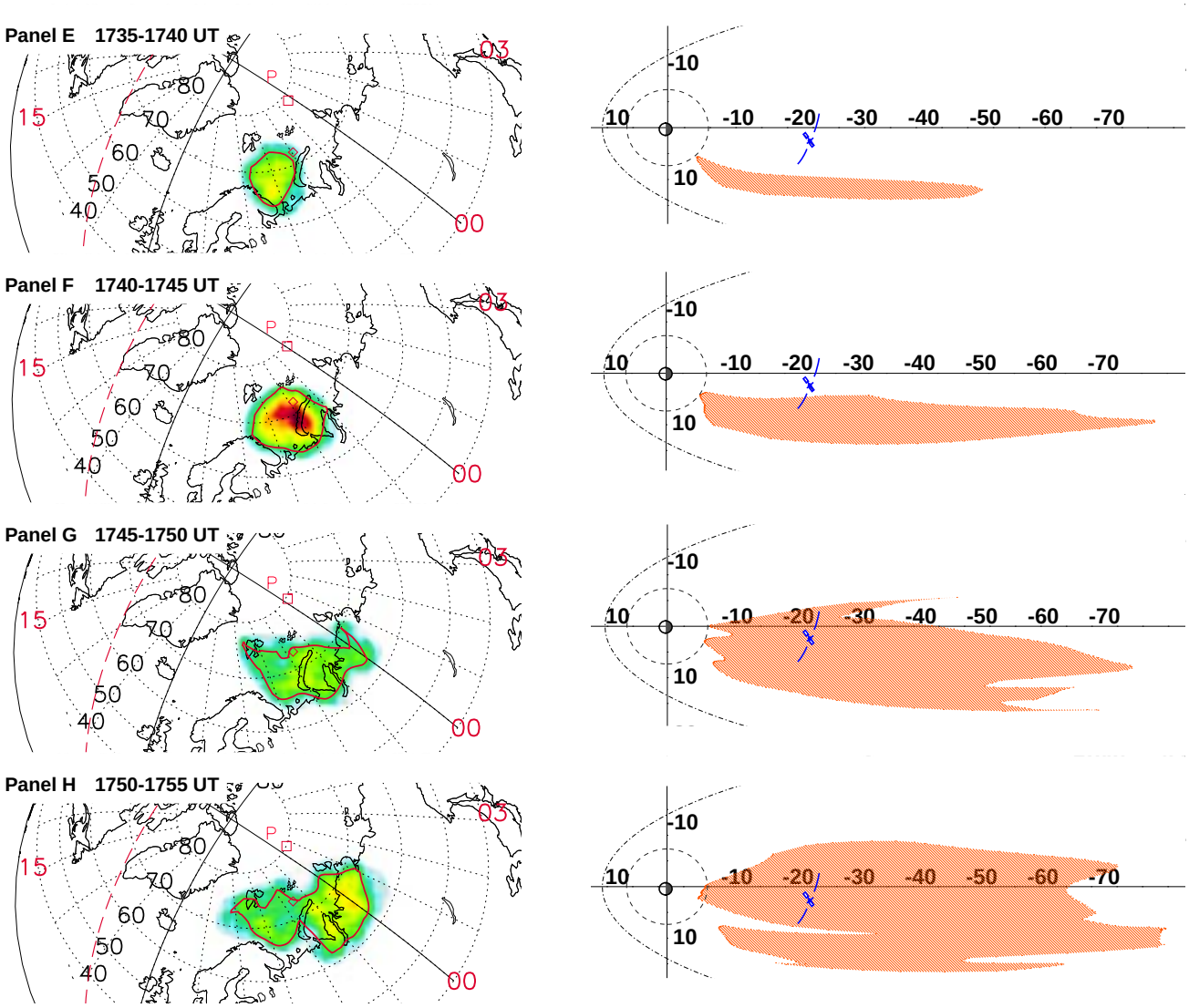

Plate 2 (continued)

The ground magnetic signatures at this stage indicate a downward FAC around 0100 MLT and an upward FAC around 2000 MLT, the latter moving rapidly westward. The positive H component in the northern hemisphere stations VAL, FUR, WNG, NCK, and HEL suggests that these stations are now inside the SCW. Furthermore, the D component at AMS, PAF, and CZT turns positive sequentially, which indicates that the upward FAC is moving westward.

The breakup is also clearly visible in the UV images in the same region as the X-ray precipitation is observed. The UV emission is also much more intense and explosive than during the first onset.

3.6. After 1736 UT

From the sequence of PIXIE images in Plate 2 (Plates 2f, 2g, and 2h) we see the precipitating region expands both westward and eastward. This is consistent with the azimuthal expansion of the current wedge in the magnetosphere.

The reentry of Geotail into the plasma sheet around 1746 UT can be identified both from the enhanced flux and the magnetic field depression (Plate 1). Note that the azimuthal directional distribution of ions shows a pronounced earthward flow of ions after 1750 UT. We therefore believe that the reconnection site (X line) has moved tailward of Geotail at this stage. The field line mapping in Plate 2g shows that the azimuthal expansion of the source region engulfs both Geotail and SC 1994-084 at 1745 - 1750 UT. This is consistent with the observation of earthward flow at Geotail and the observation of the current wedge at 1749 UT in the ion measurements at SC 1994-084 (Figure 3). The recovery phase of the substorm begins about 1755 - 1757 UT, which can be seen from X-ray fluxes in Figure 3 and the ground magnetic measurements in Figure 4.

4. Interpretation

The proposed scenario to explain the combined observations from Polar, Geotail, particle measurements at geosynchronous orbits and ground-based magnetometer measurements is illustrated in Figure 6. We interpret the various observations as follows:

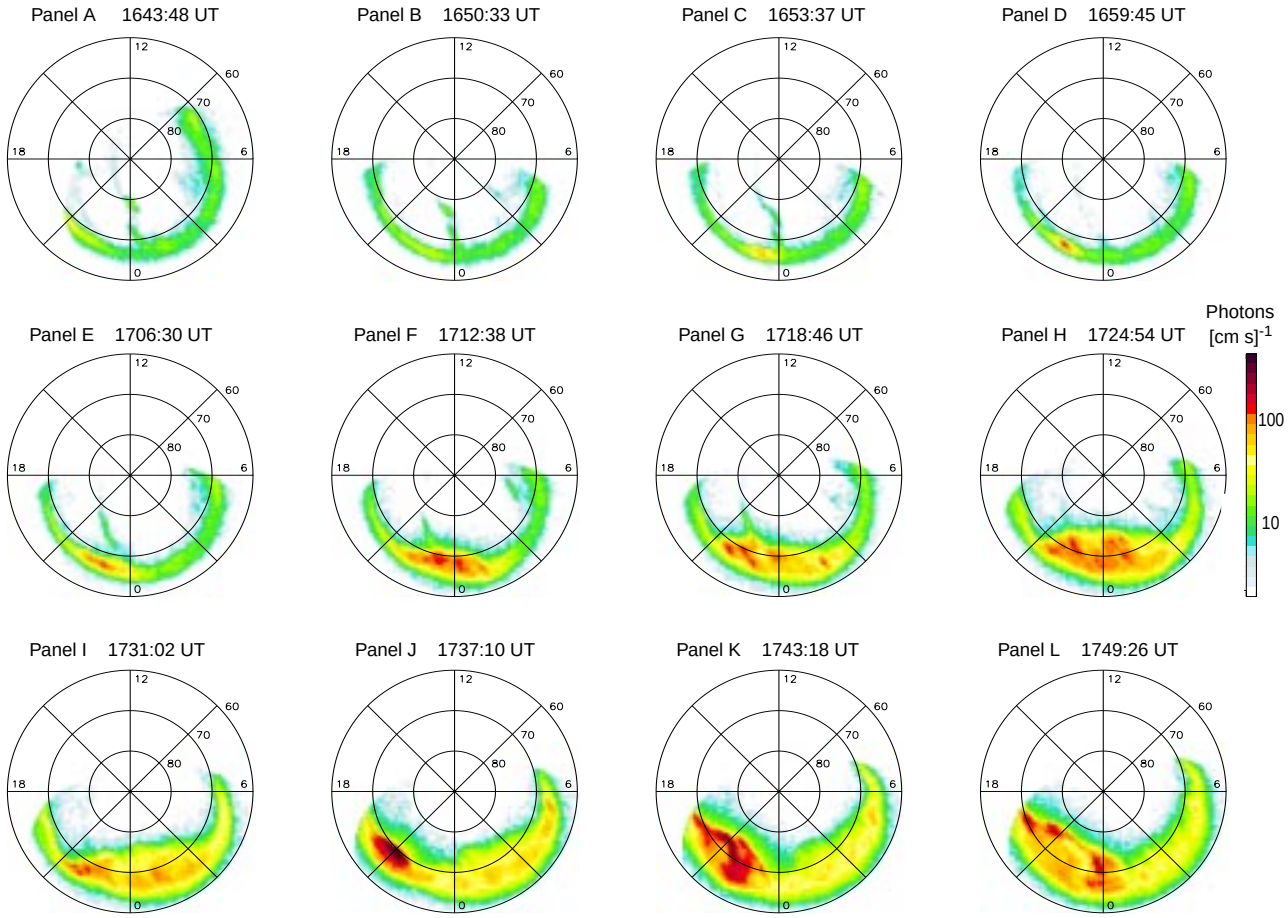

Plate 3 Sequence of 12 global UV images during the event labeled the center time of 37 s exposure time. The images show the response in the LHBL band where the emissions are primarily created by the electron impact on N_2. The first onset is seen in Plate 3e, while the second, more intense breakup further west is seen in Plate 3j. Note that a logarithmic scale and CGM grid have been used.

4.1. Prior to 1650 UT

Geotail is situated below the central plasma sheet. HEP-LD observes a fairly low but isotropic particle flux. The magnetic field indicates a stretched tail configuration which exceeds the model field during such geomagnetic conditions. Enhanced magnetic field and tail stretching are often observed during the growth phase of substorms. Some reports [e.g., *Kokubun and McPherron*, 1981] have pointed out that the growth phase associated magnetic field stretching is even more pronounced during storm periods.

Although the B_Z IMF is close to zero, the ε parameter is above the substorm threshold level, primarily due to the large solar wind velocity. However, the amount of energy stored in the magnetotail prior to the first onset at 1704 UT is low compared to the second onset at 1736 UT.

4.2. At 1654 UT

A small flux rope is launched as a result of enhanced reconnection earthward of Geotail. The magnetic signature with a "clean" bipolar B_Z and a pronounced core field in B_Y suggests that the structure resembles a closed magnetic loop rather than just branches of an X line. A principal axis analysis [see e.g., *Sonnerup and Cahill*, 1967] performed on the magnetic signatures confirms the quality of the fluxrope. Prior to this, from 1640 UT, PIXIE observes weak but distinct increases in the fluxes within the previously defined reference area. This indicates that there is some energy deposition of energetic electrons into the ionosphere. We do not know the location of the source region in the magnetosphere as the X-ray signatures are too weak to show up in the global images. However, we observe a brightening of the UV oval - another typical growth phase signature. The small changes in the electron fluxes at geosynchronous orbit indicate a displacement of the particle drift shells as a result of a change in the magnetic field configuration. However, the observations do not show any energization or injection of new particles at geosynchronous orbit at this stage. There are no signatures of field-aligned currents or Pi2 pulsations in the ground magnetic measurements. The UV intensification at 1654 UT may therefore be interpreted as a response to the reconnection event combined with the existing weak precipitation related to a stretching of the tail and subsequent particle scattering at the earthward boundary of the plasma sheet [*Sergeev et al.*, 1983].

4.3. First Onset at 1704 UT

A larger flux rope passes above Geotail ($B_X < 0$). The strong flux of tailward streaming ions observed at Geotail is evidence for

a particle source (i.e., X line or reconnection site) still operating earthward of Geotail. The magnetic field signatures are quite chaotic, and do not indicate either a closed loop or pure helical field lines.

The X-ray measurements show a new small enhancement at this time, indicating some energetic precipitation. From about 1706 UT, the UV images show an azimuthally and northward expanding bulge. We interpret this as a consequence of the first onset at 1704 UT, where the onset time was determined from the pulsation measurements at Sodankylä. The lack of any major X-ray enhancement shows that the substorm is dominated by precipitation of soft electrons. This picture is further supported by plasma data from Geotail and particle measurements from geosynchronous orbit; There is an increase in the flux of low-energy plasma (data not shown) while the energetic particle measurements at geosynchronous orbit (see Figure 3) show a recovery to the level it had prior to 1650 UT. Note that this recovery signature is quite different from the substorm injection process; there is no energization or injection of new particles. Because of the strong radial gradients in energetic particle fluxes, even small changes in the magnetic field configuration can result in large changes of the flux observed.

The substorm current wedge determined from midlatitude and low-latitude magnetic data correlates well with UV features. The downward FAC is located at eastward edge of the UV feature and the upward FAC is located at the westward edge of the UV feature.

The onset may be related to the abrupt northward turning of the IMF B_Z observed by Wind ~1648 UT. The time delay of 16 min is within reasonable agreement with the expected propagation delay between Wind and the central plasma sheet.

An important consequence of the first onset and the associated precipitation is that the conductivity in the upper ionosphere is enhanced. The event may thus also act as a preconditioner for the following onset.

The low flux observed at Geotail after 1712 UT is almost similar to dropout periods often associated with plasma sheet thinning [*Pulkkinen et al.*, 1992]. The low flux combined with a magnetic field near lobe-strength suggests that Geotail is now located below the separatrix. Note that B_Z has a weak negative value prior to 1723 UT and a weak positive value after 1723 UT. Assuming that the large scale plasma sheet is nearly aligned with the XY GSM plane, we conclude that the center of reconnection site passed above Geotail ~1723 UT.

4.4. At 1720 UT

At PIXIE, a rapid and short-lived increase in the X-ray flux is observed. The short-lived increase seems to take place at the poleward edge of the existing UV precipitation area. Mapping of the precipitation area shows that the magnetospheric source is located tailward of Geotail (see Plate 2b). This increase of the energetic precipitation may therefore be related to a partial disruption of the tail current tailward of Geotail. The current disruption does not appear to be strong enough to cause the dipolarization and the subsequently injection of the energetic particles. Still, the short-lived energetic precipitation, penetrating deep into the ionosphere, will probably cause further enhancement of the E layer conductivity [*Rees*, 1963; *Vondrak and Robinson*, 1985].

Geotail is still outside the plasma sheet and does not see any earthward particle flow. At geosynchronous orbit, a small enhancement in the proton flux around 0.4 LT and a sudden drop in the electron flux at 2200 LT are observed, but there are no distinct injection like signatures. This may indicate that the central plasma sheet (CPS) in the source region is isolated from the plasma sheet further earthward as illustrated in Figure 6. The plasma sheet boundary layer (PSBL), on the other hand, is still not isolated. Information from the source area in the distant tail may therefore propagate into the high-latitude ionosphere where the resulting precipitation is detected by PIXIE.

In the UV images, which primarily reflect the soft precipitation, a quite different development of the substorm is seen. Here, the existing bulge continues to expand northward and azimuthally. Consistently with the expansion of the UV features the inferred downward FAC move eastward, while the upward FAC moves westward.

4.5. Second Onset at 1736 UT

Major parts of the cross tail current sheet well earthward of Geotail disrupts and the magnetic field dipolarizes. An enhanced inductive electric field caused by the rapid magnetic field collapse causes an energization and injection of energetic particles. The injection front is observed at SC 1991-080 and SC 1994-084 around 1736 UT. The increased particle population at geosynchronous altitude is also observed as a faint drift echo at SC 1990-095 (not shown) located in the afternoon sector. The onset seems to be correlated with the rapid northward turning of the IMF B_Z observed at 1723 UT (delay time 13 min).

4.6. After 1736 UT

At PIXIE and UVI, the expansion phase is seen as a rapid intensification and expansion of the precipitation area. The current wedge derived from the ground magnetic perturbations seems to be well correlated with the UV features. Both UV and the ground magnetic observations indicate a westward motion. Similarly, the eastward expansion of the energetic precipitation seen as X rays correlates well with the expansion of the injection front as the mapping results indicate. The active region moves eastward and poleward as a result of the azimuthal and radial (primarily tailward) expansion of the current wedge. The increased flux of ions observed at SC 1994-084 at 1749 UT can probably be related to the azimuthal expansion of the current wedge. Geotail observes increased flux of ions at ~1750 UT when the current wedge has expanded eastward to the position of the spacecraft.

5. Discussion

During the investigated event, two onsets can be identified; 1704 and 1736 UT. In addition, there is a transient energetic precipitation event at 1720 UT. The first onset involves predominantly low-energy electrons, while the second also includes the energetic electrons.

5.1. The First Onset at 1704

The first onset at 1704 UT may be related to the northward turning IMF B_Z observed at 1648 UT. The delay time of 16 min is in agreement with the expected delay time of 10 - 16 min [*Sergeev et al.*, 1986; *Kan et al.*, 1991].

It is interesting to note that this substorm displays different characteristics depending on the energy range we examine. The soft precipitation seen in the global UV images (Plates 3e-3i) display an entire substorm development, while the energetic precipitation depicted by PIXIE only shows a transient and spatially limited event. The source region for the soft precipitation

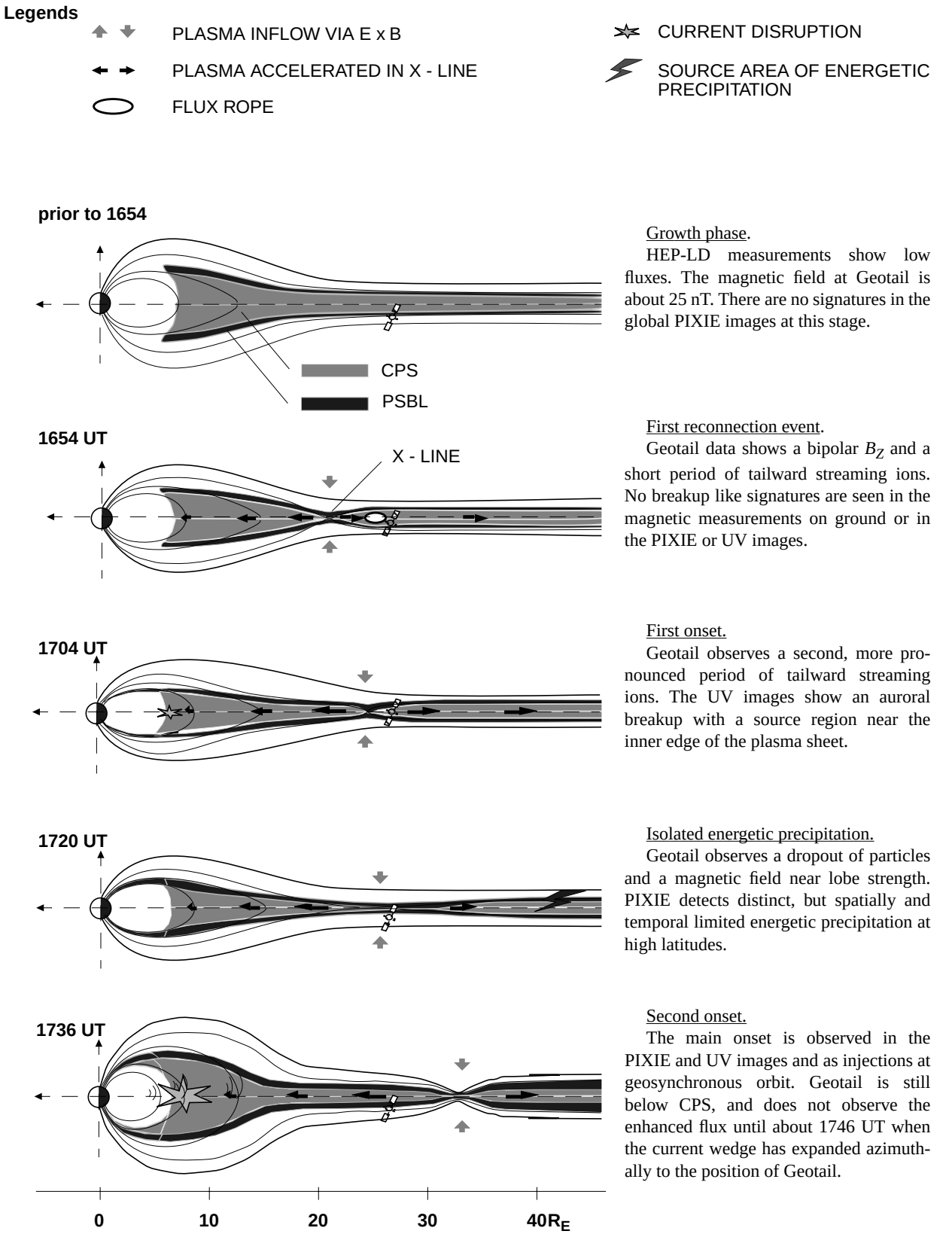

Growth phase.
HEP-LD measurements show low fluxes. The magnetic field at Geotail is about 25 nT. There are no signatures in the global PIXIE images at this stage.

First reconnection event.
Geotail data shows a bipolar B_Z and a short period of tailward streaming ions. No breakup like signatures are seen in the magnetic measurements on ground or in the PIXIE or UV images.

First onset.
Geotail observes a second, more pronounced period of tailward streaming ions. The UV images show an auroral breakup with a source region near the inner edge of the plasma sheet.

Isolated energetic precipitation.
Geotail observes a dropout of particles and a magnetic field near lobe strength. PIXIE detects distinct, but spatially and temporal limited energetic precipitation at high latitudes.

Second onset.
The main onset is observed in the PIXIE and UV images and as injections at geosynchronous orbit. Geotail is still below CPS, and does not observe the enhanced flux until about 1746 UT when the current wedge has expanded azimuthally to the position of Geotail.

Figure 6. Development in the midtail area during the event. At 1720 UT, the tailward part of the central plasma sheet (CPS) may become isolated from the inner part of the CPS. The reconnection site (X line) will prevent any exchange of information within the CPS between the two regions. However, the plasma sheet boundary layer (PSBL) has not yet been pinched off; information from the distant tail may therefore propagate to the high-latitude ionosphere.

observed in the UV images is clearly earthward of Geotail, probably close to the inner edge of the plasma sheet, whereas the energetic precipitation maps to a source area tailward of Geotail. The substorm is neither very intense nor very explosive, and there are no distinct injections at geosynchronous orbit. The low-energy input from the solar wind prior to this onset can account for the weak and slow nature of this onset.

The persisting precipitation area observed in the UV images expands poleward, enhancing at the same time and at the same location as the transient energetic precipitation occurs. The precipitation in the entire region will account for a buildup of conductivity in the ionosphere at different altitudes according to the energy differences. Such a preconditioning helps the ionosphere to support and close the field-aligned currents resulting from the current diversion in the magnetosphere.

5.2. The Second Onset at 1736 UT

The global PIXIE (and UV) images demonstrate that the breakup at 1736 UT, which includes energetic injection and precipitation, takes place on the equatorward western edge of the existing precipitation area. Although magnetic field line mapping during such disturbed conditions is subject to large uncertainties, the source area of the auroral breakup locates to a position well earthward of Geotail, possibly close to geosynchronous orbit.

Owing to a large negative IMF B_Z prior to this onset a large amount of energy has been transferred into the magnetosphere for ~20 min prior to this onset. The larger energy input may account for the stronger and more explosive nature of this onset compared to the first onset.

The current wedge derived from ground magnetic measurements correlates very well with the features of soft precipitation, while the energetic precipitation seems to correlate very well with the injection signatures from Geotail and LANL.

Although the revised NENL models [e.g., *Shiokawa et al*., 1998] does not rely on any external trigger mechanism, we note that the IMF B_Z turns rapidly northward around 1723 UT. The time delay of 13 min is in good agreement with the expected propagation times of solar wind discontinuities.

5.3. Mechanism for Substorm Onset

The observations from Geotail are consistent with the interpretation that the substorm activity is associated with magnetic reconnection in the midtail plasma sheet (~ 25 R_E) prior to both onsets. However, the PIXIE and UV images combined with the mapping results locate the source regions for the breakups to the near-Earth region.

One model which is consistent with the observations for this particular event is as following; magnetic reconnection occurs sporadically in the extremely thin plasma sheet in the near-Earth tail and midtail throughout the growth phase. Consequently, plasma will be accelerated both in the earthward and tailward direction at the reconnection site. The fact that the field lines on the earthward side connect to the Earth produces an important asymmetry. Unless rapid transport- or loss mechanisms operate, plasma ejected earthward will accumulate and the density and pressure gradients will build up.

In the unstable conditions caused by these parameters, there may be a number of candidates responsible for the current disruption and explosive onset of substorms. For the particular substorm event studied here, changes of the solar wind IMF seem to trigger the breakups.

6. Summary and Conclusion

We have presented a set of observations from a substorm event during storm time conditions on December 10, 1996. The event exhibited several of the classic substorm features, and the study provides consistent information of timing and location for the different processes which are observed:

1. Signatures of magnetic reconnection are observed in the midtail region prior to both onsets. The reconnection occurs sporadically and burst like.

2. Both onsets are manifested by electron precipitation at global scale, field-aligned currents and Pi2 pulsations.

3. The solar wind input energy prior to the first onset was low compared to the second onset. The source region of the energetic precipitation during the first onset is tailward of Geotail while the corresponding source region for the soft precipitation is well earthward of Geotail.

4. The second onset includes both soft and energetic electrons. The difference in solar wind input energy prior to the two events can probably account for the different nature of the two onsets.

5. Both onsets appear to be triggered externally by the northward turning of the IMF B_Z.

6. The source region expands both azimuthally and radially. The expansion is reflected in the precipitation area and ground magnetic perturbations.

The study presented here provides support to many of the key elements of the revised NENL model; reconnection around 25 R_E generates fast earthward plasma flow which is detected by Geotail. We do not have any direct observations of the flow braking and diversion process thought to take place at the boundary between dipolar-like and tail-like magnetic field. In the revised NENL model, the field-aligned currents are assumed to be a result of this braking process. The observed Pi2 pulsations may be a consequence of compressional pulses as postulated by the NENL model, although we do not have any observations to confirm this.

The NENL model can not account for all of the observations during the substorm event studied. The explosive nature of the onset and the close relation between the onsets and solar wind changes indicate that some kind of triggering mechanism is involved. Furthermore, individual features like, e.g., the transient precipitation event seen during this particular substorm does not easily fit into any standard model.

The event demonstrates the potential of multipoint observations provided by the ISTP program. Regions of geospace believed to be vital for substorm activity were monitored. The input energy from the solar wind were observed by the Wind spacecraft, while the Geotail and LANL satellites provided measurements from different regions of the magnetosphere. Finally, the global auroral precipitation were observed by the Polar spacecraft.

Acknowledgements. This study was partly supported by the Norwegian Research Council (NFR) and the German Space Agency (DARA). We acknowledge the use of data from the Wind Solar Wind Experiment (PI: K.Ogilvie), Wind Magnetic Field Experiment (PI: R.Lepping), Wind 3D Plasma Analyzer (PI: R.Lin) and the IMAGE Magnetometer Network (PI: A.Viljanen). Magnetic pulsation data were provided by J. Kultima, Sodankylä Geophysical Observatory. The authors thank M. Jellestad, E. Thorsen and F. Both for data processing.

Michel Blanc thanks Hannu Koskinen and Robert L. McPherron for their assistance in evaluating this paper.

References

Akasofu, S.-I., The development of the auroral substorm, *Planet. Space Sci., 12*, 273–282, 1964.

Akasofu, S.-I., Energy coupling between the solar wind and the magnetosphere, *Space Sci. Rev., 28*, 121–190, 1981.

Angelopoulos, V., V. A. Sergeev, F. S. Mozer, K. Tsuruda, S. Kokubun, T. Yamamoto, R. Lepping, G. Reeves, and E. Friis-Christensen, Spontaneous substorm onset during a prolonged period of steady, southward interplanetary magnetic field, *J. Geophys. Res., 101*, 24,583–24,598, 1996.

Baker, D. N., T. I. Pulkkinen, V. Angelopoulos, W. Baumjohann, and R. L. McPherron, Neutral line model of substorms: Past results and present view, *J. Geophys. Res., 101*, 12,975–13,010, 1996.

Berger, M. J., and S. M. Seltzer, Bremsstrahlung in the atmosphere, *J. Atmos. Terr. Phys., 34*, 85–108, 1972.

Doke, T. et al., The energetic particle spectrometer HEP onboard the GEOTAIL spacecraft, *J. Geomagn. Geoelectr., 46*, 713–733, 1994.

Erickson, K. N., R. L. Swanson, R. J. Walker, and J. R. Winckler, A study of magnetospheric dynamics during auroral electrojet events by observation of energetic electron intensity changes at geosynchronous orbit, *J. Geophys. Res., 84*, 931–942, 1979.

Henderson, M. G., G. D. Reeves, R. D. Belian, and J. S. Murphree, Observations of magnetospheric substorms occurring with no apparent solar wind/IMF trigger, *J. Geophys. Res., 101*, 10,773–10,791, 1996.

Hones, E. W., The magnetotail: Its generation and dissipation, in *Physics of Solar Planetary Environments*, edited by D. J. Williams, pp. 559–591, AGU, Washington D.C., 1976.

Hones, E. W., Substorm processes in the magnetotail: Comments on "on hot tenous plasmas, fireballs, and boundary layers in the Earth's magnetotail" by L. A. Frank, K. L. Ackerson and R. P. Lepping, *J. Geophys. Res., 82*, 5633–5640, 1977.

Imhof, W. L. et al., The Polar Ionospheric X-ray Imaging Experiment (PIXIE), *Space Sci. Rev., 71*, 385–408, 1995.

Kan, J. R., L. Zhu, A. T. Y. Lui, and S.-I. Akasofu, A magnetosphere-ionosphere coupling theory of substorms including magnetotail dynamics, in *Auroral Physics*, edited by C.-L. Meng, M. J. Rycroft, and L. A. Frank, pp. 311–321, Cambridge Univ. Press, New York, 1991.

Kettmann, G., and P. W. Daly, Detailed determination of the orientation and motion of the plasma sheet boundary layer using energetic protons on ISEE 1 and 2: Waves, curves and flapping, *J. Geophys. Res., 93*, 7376–7385, 1988.

Kokubun, S., and R. L. McPherron, Substorm signatures at synchronous altitudes, *J. Geophys. Res., 86*, 11,265–11,277, 1981.

Kokubun, S., R. L. McPherron, and C. T. Russell, Triggering of substorms by solar wind discontinuities, *J. Geophys. Res., 82*, 74–86, 1977.

Lepping, R. P. et al., The WIND magnetic field investigation, *Space Sci. Rev., 71*, 207–229, 1995.

Lui, A. T. Y., A synthesis of magnetospheric substorm models, *J. Geophys. Res., 96*, 1849–1856, 1991.

Lui, A. T. Y., Current disruption in the Earth's magnetosphere: Observations and models, *J. Geophys. Res., 101*, 13,067–13,088, 1996.

Lyons, L. R., A new theory of magnetospheric substorms, *J. Geophys. Res., 100*, 19,069–19,081, 1995.

Lyons, L. R., Evidence suggests external triggering of substorms, *Eos Trans. AGU, 77*, 87, 1996.

McPherron, R. L., C. T. Russell, and M. P. Aubrey, Satellite studies of magnetospheric substorms on August 15, 1968, 9. Phenomenological model for substorms, *J. Geophys. Res., 78*, 3131–3149, 1973.

Mukai, T., S. Machida, Y. Saito, M. Hirahara, T. Terasawa, N. Kaya, T. Obara, M. Ejiri, and A. Nishida, The Low Energy Particle (LEP) experiment onboard the GEOTAIL satellite, *J. Geomagn. Geoelectr., 46*, 669–692, 1994.

Ogilvie, K. W. et al., SWE, A comprehensive plasma instrument for the WIND spacecraft, *Space Sci. Rev., 71*, 55–77, 1995.

Ohtani, S., S. Kokubun, R. Nakamura, R. C. Elphic, C. T. Russell, and D. N. Baker, Field-aligned current signatures in the near-tail region, 2, Coupling between the region 1 and the region 2 systems, *J. Geophys. Res., 95*, 18,913–18,927, 1990.

Pulkkinen, T. I., D. N. Baker, D. G. Mitchell, R. L. McPherron, C. Y. Huang, and L. A. Frank, Global and local current sheet thickness estimates during the late growth phase, in *Substorms ICS-1*, edited by C. Mattok. *Eur. Space Agency Spec. Publ., ESA SP-335*, 131–135, 1992.

Rees, M. H., Auroral ionization and excitation by incident energetic electrons, *Planet. Space Sci., 11*, 1209–1218, 1963.

Richardson, I. G., and S. W. H. Cowley, Plasmoid associated energetic ion burst in the deep geomagnetic tail: Properties of the boundary layer, *J. Geophys. Res., 90*, 12,133–12,158, 1985.

Richardson, I. G., S. W. H. Cowley, E. W. Hones, and S. J. Bame, Plasmoid-associated energetic ion bursts in the deep geomagnetic tail: Properties of plasmoid and the postplasmoid plasma sheet, *J. Geophys. Res., 92*, 9997–10,013, 1987.

Richardson, I. G., C. J. Owen, S. W. H. Cowley, A. B. Galvin, T. R. Sanderson, M. Scholer, J. A. Slavin, and R. D. Zwickl, ISEE 3 observations during the the CDAW 8 interval: Case studies of the distant geomagnetic tail covering a wide range of geomagnetic activity, *J. Geophys. Res., 94*, 15,189–15,220, 1989.

Robinson, R. M., and R. R. Vondrak, Validation of techniques for space based remote sensing of auroral precipitation and its ionospheric effect, *Space Sci. Rev., 69*, 331–407, 1994.

Scholer, M., G. Gloeckler, D. Hovestadt, B. Klecker, and F. M. Ipavich, Characteristics of plasmoidlike structures in the distant magnetotail, *J. Geophys. Res., 89*, 8872–8876, 1984a.

Scholer, M., G. Gloeckler, B. Klecker, F. M. Ipavich, D. Hovestadt, and E. J. Smith, Fast moving plasma structures in the distant magnetotail, *J. Geophys. Res., 89*, 6717–6727, 1984b.

Sergeev, V. A., E. M. Sazhina, N. A. Tsyganenko, J. Å. Lundblad, and F. Søraas, Pitch angle scattering of energetic protons in the magnetotail current sheet as the dominant source of their isotropic precipitation into the nightside ionosphere, *Planet. Space Sci., 31*, 1147–1155, 1983.

Sergeev, V. A., N. P. Dmitrieva, and E. S. Bakova, Triggering of substorm expansion by the IMF directional discontinuities: Time delay analysis, Planet. Space Sci., 34, 1109–1118, 1986.

Shiokawa, K. et al., High-speed ion flow, substorm current wedge, and multiple Pi 2 pulsations, *J. Geophys. Res., 103*, 4491–4507, 1998.

Slavin, J. A. et al., CDAW 8 observations of plasmoid signatures in the geomagnetic tail: An assessment, *J. Geophys. Res., 94*, 15,153–15,175, 1989.

Slavin, J. A., C. J. Owen, M. M. Kuznetsova, and M. Hesse, ISEE 3 observations of plasmoids with flux rope magnetic topologies, *Geophys. Res. Lett., 22*, 2061–2064, 1995.

Sonnerup, B. Ö., and L. J. Cahill, Magnetopause structure and attitude from Explorer 12 observations, *J. Geophys. Res., 72*, 171–183, 1967.

Spence, H. E., The what, where, when, and why of magnetospheric substorm triggers, *Eos Trans. AGU, 77*, 81, 1996.

Torr, M. R. et al., A far ultraviolet imager for the international solar-terrestrial physics mission., *Space Sci. Rev., 71*, 329–383, 1995.

Tsyganenko, N. A., Modelling the Earth's magnetospheric magnetic field confined within a realistic magnetopause, *J. Geophys. Res., 100*, 5599–5612, 1995.

Vondrak, R. R., and R. Robinson, Inference of high-latitude ionization and conductivity from AE-C measurements of auroral electron fluxes, *J. Geophys. Res., 90*, 7505–7512, 1985.

Wilken, B. et al., RAPID: The imaging energetic particle spectrometer on Cluster, in *Cluster: Mission, Payload and Supporting Activities*, edited by W. R. Burke, pp. 185–218, ESA Publ. Div., ESTEC, Noordwijk, Netherlands, 1993.